Relative effect of host versus non-host vegetation structure on for-

₂ est insect severity depends on climatic water deficit

- Michael J. Koontz^{1,2,*}, Andrew M. Latimer^{1,2}, Leif A. Mortenson³, Christopher J. Fettig³, Constance I.
- ⁴ Millar⁴, Malcolm P. North^{1,2,5}
- ⁵ Graduate Group in Ecology, University of Californa, Davis, CA, USA
- ⁶ Department of Plant Sciences, University of California, Davis, CA, USA
- ⁷ ³USDA Forest Service, Pacific Southwest Research Station, Placerville, CA, USA
- ⁸ ⁴USDA Forest Service, Pacific Southwest Research Station, Albany, CA, USA
- ⁵ USDA Forest Service, Pacific Southwest Research Station, Davis, CA, USA
- *Correspondence: michael.koontz@colorado.edu
- Date report generated: March 11, 2019

12 Abstract

- Forest insects are a primary mortality agent of trees in Sierra Nevada mixed-conifer forests. The recent hot
- drought from 2012 to 2015 led to massive tree die-off throughout the state of California, and especially in the
- 15 Sierra Nevada.

16 Introduction

- Aggressive bark beetles dealt the final blow to many of the nearly 150 million trees killed in the California
- drought of 2012 to 2015 and its aftermath (USDAFS 2019). A harbinger of climate change effects to come,
- 19 high temperatures exacerbating the extreme drought led to tree mortality events of unprecedented size in the
- driest, densest forests across the state (Millar and Stephenson 2015; Young et al. 2017). A century of fire
- suppression policy has enabled forests to grow unchecked into dense stands, which increases water stress on
- trees and makes them more vulnerable to bark beetle attack (Fettig 2012; North et al. 2015).
- 23 Previous studies show that bark beetles thrive in denser forests (Fettig 2012), but density is often a coarse
- 24 gauge of the size and spatial distribution of trees- the forest structure- with which bark beetles interact
- ²⁵ (Raffa et al. 2008).
- 26 Recent research has shown a strong link between complex forest structure and forest resilience, but measuring
- 27 this complexity generally requires expensive equipment or labor-intensive field surveys (Larson and Churchill
- ²⁸ 2012; Kane et al. 2014). These barriers restrict survey frequency and extent, which limits insights into

phenomena like bark beetle outbreaks that rapidly emerge over weeks to months but have long-lasting effects
 on forest conditions.

Further, the clear and vast latitudinal gradient of mortality challenges our ability to simultaneously consider how environmental conditions may interact with local forest structure to produce patterns of insect activity.

along a strong south to north latitudinal gradient (Young et al. 2017; USDAFS 2019). Latitudinal and elevational gradients in the intensity of bark beetle activity during the recent California drought provide unique opportunities for a postmortem analysis of a major tree die off and how intersecting forces of forest structure and environmental conditions affect disturbance dynamics. Quantitative, fine-scale measures of tree condition across these geographic gradients will enable broad-scale assessment of forest structure as well as the intensity of western pine beetle-induced tree mortality. Combined, these measurements can better our understanding of how complex forest structure affects insect disturbance, and vice versa, across the Sierra Nevada. Sound forest management requires a better understanding of the relationships between forest spatial structure, environmental conditions, and disturbance, which ultimately depends on accurate measurement of forest structure at appropriate spatial scales.

Forests in California's Sierra Nevada region are characterized by regular bark beetle disturbances that interact with forest structure. Bark beetles shape forest structure as they sporadically kill weakened trees under normal conditions, or wide swaths of even healthy trees under outbreak conditions. Forest structure also strongly influences bark beetle activity. Low-density forests are less prone to bark beetle attacks, but resolving the mechanism underlying this observation requires a more nuanced view of forest structure. For instance, a low-density forest may resist attack because its trees are in smaller clumps with greater average tree vigor, or because its wider canopy openings disrupt pheromone signaling between beetles (Fettig 2012). Thus, it remains poorly understood how complex forest structure affects and is affected by bark beetle activity.

Forest spatial structure, the size and distribution of trees in the forest, is thought to be a key determinant of forest resilience. To date, much of the work on Sierra Nevada forest resilience focuses on stem density, which belies the complexity of forest structure and how it interacts with disturbance. However, complex forest structure is challenging to quantify, as it requires labor-intensive field surveys (e.g., to generate stem maps) or highly specialized, expensive equipment (e.g., LiDAR). Small, unmanned aerial systems (sUAS) enable fast and relatively cheap remote imaging over dozens of hectares of forest, which can be used to determine both forest structure and tree condition at the individual tree scale. Implementing photogrammetry on the collected images can provide a rich picture of the complex, 3-dimensional forest structure to which bark beetles respond, and equipping the sUAS with a multispectral sensor will allow calculation of vegetation

- indices (e.g., NDVI) commonly used to assess tree condition.
- 61 Climate change mitigation strategies emphasize reducing tree densities (North et al. 2015; Young et al. 2017),
- but understanding the optimal scale and pattern of tree distribution that can mitigate bark beetle outbreaks
- 63 will be vital for predicting how California forests may respond to these interventions. This project investigates
- this relationship with the following research questions:
- 1. How does local host tree density affect the severity of western pine beetle disturbance?
- 2. How does total tree density affect the severity of western pine beetle disturbance?
- 3. How does environmentally-driven tree moisture stress affect the severity of western pine beetle disturbance?
- 4. Do the effects of forest structure and environmental condition on western pine beetle disturbance interact?
- ⁷¹ We used ultra-high resolution remote sensing data from a small, unhumanned aerial system (sUAS, aka
- drone) over a network of 32 sites in the Sierra Nevada spanning 1000m of elevation and 350km of latitude and
- covering a total of 9 square kilometers of forest to ask how fine-scale forest structure affected the probability
- of tree mortality during the cumulative mortality event of

75 Methods

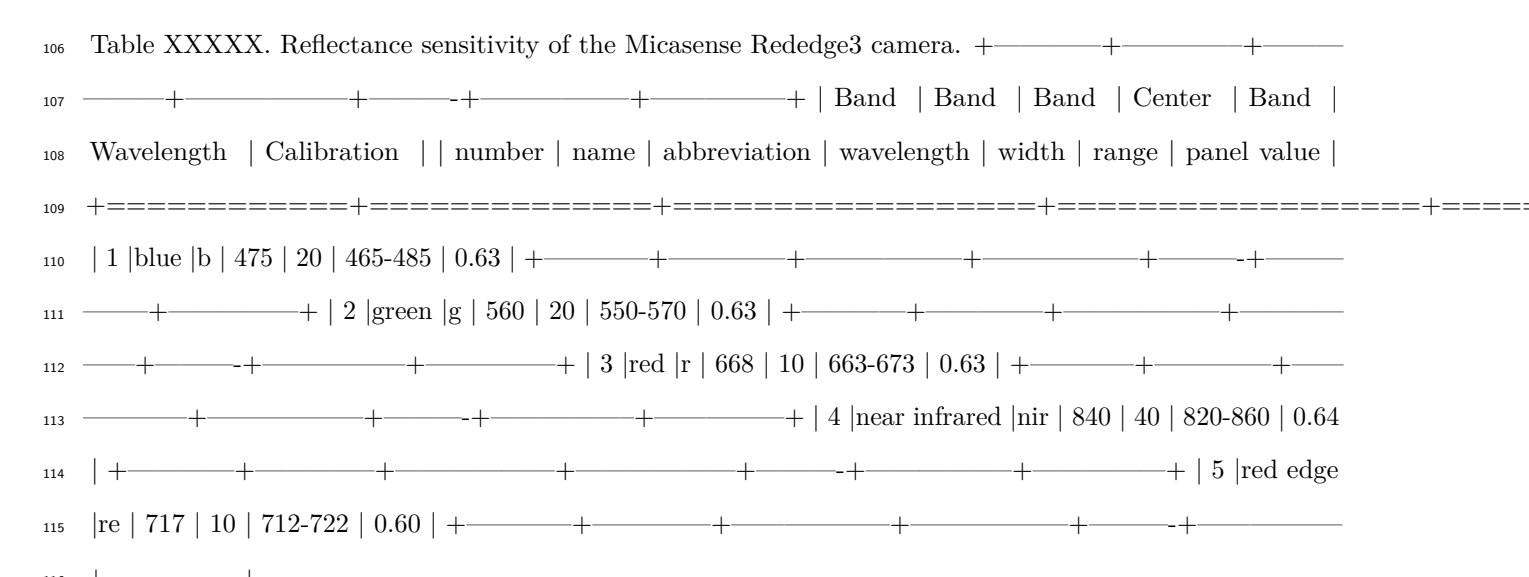
76 Study system

- 77 The study sites comprise mostly ponderosa pine trees, *Pinus ponderosa*, whose primary bark beetle predator
- 78 in California is the western pine beetle (WPB), Dendroctonus brevicomis. The WPB is an aggressive bark
- beetle, meaning it must attack and kill live trees in order to successfully reproduce (Raffa et al. 2008).
- ⁸⁰ Pioneer WPBs disperse to a new host tree, determine the host's susceptibility to attack, and use pheromone
- 81 signals to attract other WPBs. The attracted WPBs mass attack the tree by boring into its inner bark,
- laying eggs, and dying, leaving their offspring to develop inside the doomed tree before themselves dispersing
- 83 (Raffa et al. 2008). Small WPB populations prefer weakened trees but large populations can overwhelm
- the defense mechanisms of even healthy trees. Successful attacks on large, healthy trees are boons to bark
- beetle fecundity and trigger outbreaks in which populations explode and massive tree mortality occurs. In
- ⁸⁶ California, the WPB can have 3 generations in a single year giving it a greater potential to spread rapidly
- through forests than its more infamous congener, the mountain pine beetle, *Dendroctonus ponderosa* (MPB).
- ⁸⁸ We built our study on 180 vegetation monitoring plots at 36 sites established between 2016 and 2017 (Fettig

et al. 2019). These established plots are located in beetle-attacked, mixed-conifer forests across the Eldorado,
Stanislaus, Sierra and Sequoia National Forests across an elevation gradient (3000-4000 feet, 4000-5000 feet,
and 5000+ feet above sea level) and have variable forest structure and disturbance history. Plot locations
were selected specifically in areas with >40% ponderosa pine basal area and >10% ponderosa pine mortality.
The 0.04ha circular plots are clustered along transects in groups of 5, with between 80 and 200m between
each plot. All trees within the plot were assessed as dead or alive. The stem location of all trees was mapped
relative to the center of each plot using azimuth/distance measurements. Tree identity to species and diameter
at breast height (dbh) were recorded if dbh was greater than 6.35cm. During the spring and early summer of
2018, all field plots were revisited to assess whether dead trees had fallen.

98 Instrumentation

Imagery was captured using a DJI Zenmuse X3 RGB camera (DJI 2015a) and a Micasense RedEdge3 5-band multispectral camera (Micasense 2015). We mounted both of these instruments simultaneously on a DJI Matrice 100 aircraft (DJI 2015b) using the DJI 3-axis stabilized gimbal for the Zenmuse X3 camera and a Micasense angled fixed mount for the RedEdge3 camera. The gimbal and the angled fixed mount ensured both instruments were nadir-facing during image capture. Just prior or after image capture at each site, we calibrated the RedEdge3 camera by taking an image of a calibration panel on the ground in full sun with known reflectance values for each of the 5 narrow bands.



117 Flight protocol

- Image capture was conducted as close to solar noon as possible to minimize shadow effects (always within 4 hours; usually within 2 hours). Prior to the aerial survey, two strips of bright orange drop cloth (~100cm x 15cm) were positioned as an "X" over the permanent monuments marking the center of the 5 field plots from Fettig et al. (2019).
- For each of the 36 sites (containing 5 plots each), we captured imagery over the surrounding ~40 hectares of forested area using north-south aerial transects. For XXXXX sites, we surveyed less surrounding area in order to maintain visual and radio communication with the aircraft during flight (Table XXXXXX).
- We preprogrammed transect paths using Map Pilot for DJI on iOS (hereafter Map Pilot) (Easy 2018). All transects tracked the terrain and their altitude remained approximately constant at 120 meters above ground level in order to maintain consistent ground sampling distance in the imagery. Ground level was based on a 1-arc-second digital elevation model (Farr et al. 2007) and we implemented terrain following using Map Pilot. For this analysis, we dropped 4 sites whose imagery was of insufficient quality to process.
- Structure from motion (SfM) processing requires highly overlapping images, especially in densely vegetated areas. We planned transects with 90% forward overlap and 90% side overlap at 100 meters below the lens. Thus, with flights being at 120 meters above ground level, we achieved slightly higher than 90/90 overlap for objects 20 meters tall or shorter. Overlap values were based on focal length and field of view parameters of the Zenmuse X3 camera. Images were captured at a constant rate of 1 image every 2 seconds for both cameras. A forward overlap of 90% at 100 meters translates to a flight speed of approximately 6.3 m/s and a side overlap of 90% at 100 meters translates to transects approximately 18 meters apart. Approximately 1900 photos were captured over each 40 hectare survey area for each camera.

138 Structure from motion/Photogrammetric processing

We used structure from motion (SfM), aka photogrammetry, to generate orthorectified reflectance maps,
digital surface models, and dense point clouds for each field site. We used Pix4Dmapper Cloud to process
imagery using parameters ideal for images of a densely vegetated area taken by a multispectral camera.
For three sites, we processed the RGB and the multispectral imagery in the same project to enhance the
resolution of the dense point cloud. All SfM projects resulted in a single processing "block," indicating that
all images in the project were optimized and processed together.

145 Creating canopy height models

We classified each survey area's dense point cloud into "ground" and "non-ground" points using a cloth simulation filter algorithm (Zhang et al. 2016) implemented in the lidR (Roussel et al. 2019) package. We rasterized the ground points using the raster package (Hijmans et al. 2019) to create a digital terrain model representing the ground underneath the vegetation at 1 meter resolution. We created a canopy height model by subtracting the digital terrain model from the digital surface model created in Pix4Dmapper.

151 Tree detection

We tested a total of 7 automatic tree detection algorithms and a total of 177 parameter sets on the canopy 152 height model or the dense point cloud to locate trees within each site (Table XXXXX; algorithm, number of parameter sets, reference). We used 3 parameter sets of a variable window filter implemented in ForestTools 154 (Plowright 2018) including the default variable window filter function in ForestTools as well as the "pines" and "combined" functions from Popescu and Wynne (2004). We used 6 parameter sets of a local maximum 156 filter implemented in lidR. We used 131 parameter sets of the algorithm from Li et al. (2012), which operates 157 on the original point cloud. These parameter sets included those from Shin et al. (2018) and Jakubowski et 158 al. (2013). We used 3 parameter sets of the watershed algorithm implemented in lide, which is a wrapper 159 for a function in the EBImage package (Pau et al. 2010). We used 3 parameter sets of ptrees (Vega et al. 160 2014) implemented in lidR (Roussel et al. 2019) and lidRplugins (Roussel 2019) and which operates on 161 the raw point cloud, without first normalizing it to height above ground level (i.e., subtracting the ground elevation from the dense point cloud). We used the default parameter set of the multichm (Evsn et al. 2015) 163 algorithm implemented in lidR (Roussel et al. 2019) and lidRplugins (Roussel 2019). We used 30 parameter sets of the experimental algorithm lmfx (Roussel 2019). 165

166 Map ground data

Each orthorectified reflectance map was inspected to locate the 5 orange "X"s marking the center of the field plots. We were able to locate 110 out of 180 field plots and were then able to use these plots for validation of automated tree detection algorithms. We used the sf package (Pebesma et al. 2019) to convert distance-from-center and azimuth measurements of each tree in the ground plots to an x-y position on the SfM-derived reflectance map using the x-y position of the orange X visible in the reflectance map as the center.

173 Correspondence of automatic tree detection with ground data

- We calculated 7 forest structure metrics for each field plot using the ground data collected by Fettig *et al.* (2019): total number of trees, number of trees greater than 15 meters, number of trees less than 15 meters, mean height of trees, 25th percentile tree height, 75th percentile tree height, mean distance to nearest tree neighbor, mean distance to 2nd nearest neighbor.
- For each tree detection algorithm and parameter set described above, we calculated the same set of 7 structure metrics within the footprint of the validation field plots. We calculated the Pearson's correlation and root mean square error (RMSE) between the ground data and the aerial data for each of the 7 structure metrics for each of the XXXXX automatic tree detection algorithms.
- For each algorithm and parameter set, we calculated its performance relative to other algorithms as whether its Pearson's correlation was within 5% of the highest Pearson's correlation as well as whether its RMSE was within 5% of the lowest RMSE. For each algorithm/parameter set, we summed the number of forest structure metrics for which it reached these 5% thresholds. For automatically detecting trees across the whole study, we selected the algorithm/parameter set that performed well across the most number of forest metrics.

187 Segmentation of crowns

- We delineated individual tree crowns with a marker controlled watershed segmentation algorithm (Meyer and Beucher 1990) using the detected treetops as markers implemented in the ForestTools package (Plowright 2018). If the automatic segmentation algorithm failed to generate a crown segment for a detected tree (e.g., often snags with a very small crown footprint), a circular crown was generated with a radius of 0.5 meters. If the segmentation generated multiple polygons for a single detected tree, only the polygon containing the detected tree was retained. Image overlap decreases near the edges of the overall flight path, which reduces the quality of the SfM processing in those areas. Thus, we excluded segmented crowns within 35 meters of the edge of the survey area.
- We used the velox package (Hunziker 2017) to extract all the pixel values from the orthorectified reflectance map for each of the 5 narrow bands within each segmented crown polygon. Per pixel, we additionally calculated the normalized difference vegetation index (NDVI; Rouse et al. (1973)), the normalized difference red edge (NDRE; Gitelson and Merzlyak (1994)), the red-green index (RGI; Coops et al. (2006)), the red edge chlorophyll index (CI[red edge]; Clevers and Gitelson (2013)), and the green chlorophyll index (CI[green]; Clevers and Gitelson (2013)). For each crown polygon, we calculated the mean value for each raw and derived reflectance band (5 raw; 5 derived).

203 Classification of trees

- We overlaid the segmented crowns on the reflectance maps from 20 sites spanning the latitudinal and elevational gradient in the study. Using QGIS, we hand classified XXXX trees as live/dead and as one of 5 dominant species in the study area (*Pinus ponderosa*, *Pinus lambertiana*, *Abies concolor*, *Calocedrus decurrens*, or *Quercus kelloggi*) using the mapped ground data as a guide.
- We used all 10 mean values of the reflectance bands for each tree crown polygon to predict whether the hand classified trees were alive or dead using a boosted logistic regression model implemented in the caret package (Kuhn 2008). For just the living trees, we similarly used all 10 reflectance values to predict the tree species using regularized discriminant analysis implemented in the caret package, which proved to have the highest accuracy for a training dataset (accuracy = XXXXX, kappa = XXXXX).
- Finally, we used these models to classify all tree crowns in the data set as alive or dead as well as the species of living trees.

215 Allometric scaling of height to basal area

We converted the height of each tree (known from the canopy height model) to its basal area. Using the tree height and diameter at breast height (DBH; breast height = 1.37m) ground data, we fit a simple linear regression to predict DBH from height for each of the 5 dominant species. Using the model-classified tree species of each segmented tree, we used the corresponding linear relationship for that species to estimate the DBH given the tree's height. We then calculated each tree's basal area, assuming no tapering from breast height.

Note on assumptions about dead trees

For the purposes of this study, we assumed that all dead trees were ponderosa pine. This is a reasonably good assumption, given that Fettig *et al.* (2019) found that XXXXX% (~90) of the dead trees in the coincident ground plots were ponderosa pine.

Rasterizing individual tree data

Because the tree detection algorithms were validated against ground data at the plot level, we rasterized the
classified trees at a spatial resolution similar to that of the ground plots (rasterized to 20m x 20m equalling
400 m²; circular ground plots with 11.35m radius equalling 404 m²). In each raster cell, we tallied: number
of alive trees, number of dead trees, number of ponderosa pine trees, number of non-ponderosa pine trees,
basal area of ponderosa pine trees, basal area of non-ponderosa pine trees.

232 Environmental data

We used climatic water deficit (CWD) (Stephenson 1998) from the 1980-2010 mean value of the basin 233 characterization model (Flint et al. 2013) as an integrated measure of temperature and moisture conditions for each cell. Higher values of CWD correspond to hotter, drier conditions and lower values correspond 235 to cooler, wetter conditions CWD has been shown to correlate well with broad patterns of tree mortality in the Sierra Nevada (Young et al. 2017). We resampled the climatic water deficit product using bilinear 237 interpolation implemented in the raster package to match the 20m x 20m spatial scale of the other variables. 238 We converted the CWD value for each cell into a z-score representing that cell's deviation from the mean 230 CWD across the climatic range of Sierra Nevada ponderosa pine as determined from XXXXX herbarium 240 records described in Baldwin et al. (2017). Thus, a CWD z-score of one would indicate that the CWD at 241 that cell is one standard deviation hotter/drier than the mean CWD across all geolocated herbarium records 242 for ponderosa pine in the Sierra Nevada.

244 Statistical model

We used a generalized additive model with a binomial response and a logit link to predict the probability
of ponderosa pine mortality within each raster cell as a function of the crossed effects of ponderosa pine
quadratic mean diameter and count added to the crossed effect of non-ponderosa pine quadratic mean
diameter and count as well as the interaction of each summand with climatic water deficit. To account for
spatial autocorrelation of the processes underlying ponderosa mortality, we included a separate smoothing
term per site of the interaction between the x- and y-position of each cell using the mgcv package (Wood et
al. 2016) with a thin plate spline basis having a dimension of 10.

52 Model checking...

$$y_{i} \sim Binom(n_{i}, \theta_{i})$$

$$logit(\theta_{i}) = \beta_{0} + \gamma_{i} +$$

$$\beta_{1}X_{cwd,i} +$$

$$\beta_{1}X_{cwd,i}(\beta_{2}X_{pipoBA,i} + \beta_{3}X_{pipoCount,i} + \beta_{4}X_{pipoBA,i}X_{pipoCount,i}) +$$

$$\beta_{1}X_{cwd,i}(\beta_{5}X_{nonpipoBA,i} + \beta_{6}X_{nonpipoCount,i} + \beta_{7}X_{nonpipoBA,i}X_{nonpipoCount,i})$$

$$\gamma_{i} \sim Norm(\mu = 0, \sigma^{2})$$

Where y_i is the number of dead ponderosa pine trees in cell i, n_i is the total number of ponderosa pine trees in cell i, θ_i is the probability of a pine tree dying in cell i, $X_{cwd,i}$ is the z-score of climatic water

deficit, $X_{pipoBA,i}$ is the centered basal area of ponderosa pine in a cell, $X_{pipoCount,i}$ is the centered number of ponderosa pine trees in a cell, $X_{nonpipoBA,i}$ is the centered total basal area of non-ponderosa pine trees in a cell, $X_{nonpipoCount,i}$ is the centered number of non-ponderosa pine trees in a cell, and γ_i is a random deviation from the log-odds of ponderosa pine mortality at mean values of ponderosa pine basal area and count, mean values of non-ponderosa pine basal area and count, and mean value of climatic water deficit across the full range of Sierra Nevada ponderosa pine. σ^2 represents the pooled variance of these random deviations.

262 Software and data availability

All data are available via the Open Science Framework. Statistical analyses were performed using the mgcv and brms packages. With the exception of the SfM software (Pix4Dmapper Cloud) and the GIS software QGIS, all data carpentry and analyses were performed using R (R Core Team 2018).

266 Results

²⁶⁷ Tree detection

We found that the experimental lmfx algorithm with parameter values of XXXXX (Roussel et al. 2019)
performed the best across 7 measures of forest structure as measured by Pearson's correlation with ground
data (Table XXXX; rows are different forest metrics, columns are correlation and RMSE).

271 Effect of local structure on western pine beetle severity

- We found a strong main effect of climatic water deficit on the probability of ponderosa pine mortality within each 20m x 20m cell. Greater climatic water deficit, indicating hotter/drier conditions, increased the probability of ponderosa pine mortality.
- We also found a strong effect of ponderosa pine basal area, accounting for the total basal area with greater ponderosa pine basal area increasing the probability of ponderosa pine mortality.
- We found a negative effect of total basal area on the probability of ponderosa pine mortality.
- $_{278}$ We found no 2-way interaction between ponderosa pine basal area and total basal area.
- We found a significant 3-way interaction between ponderosa pine basal area, total basal area, and climatic
 water deficit. In hotter, drier sites, a positive interaction between ponderosa pine basal area and total basal
 area emerges.

282 Discussion

Similarities and differences with Fettig et al. (2019)

- Fettig et al. (2019) found positive relationship between number of trees killed and: total number of trees,
- total basal area, stand density index.
- Fettig et al. (2019) found negative relationship between the proportion of trees killed and: total number of
- trees, stand density index.
- Hayes et al. (2009) and Fettig et al. (2019) found measures of host availability explained less variation in
- 289 mortality than measures of stand density.
- Negrón et al. (2009) reported positive association of probability of ponderosa pine mortality and tree density
- ²⁹¹ during a drought in Arizona.
- 292 Effect of competition may be masked because drought was so extreme Fettig et al. (2019); Floyd et al.
- ²⁹³ (2009), which is perhaps why we saw a counter-intuitive signal of increasing total basal area leading to lower
- 294 probability of ponderosa pine mortality.

295 Broader context around field plots

- ²⁹⁶ We surveyed 9 square kilometers of forest representing XXXXXX trees along a broad gradient. Site selection
- ²⁹⁷ and small plot size can influence inference. For instance, Fettig et al. (2019) reported statistically undetectable
- differences in overall mortality in their plot network across 4 national forests. By expanding the hectarage
- surveyed by a factor of 200, we detected dramatic differences in overall mortality.
- This is about more than sample size. This is also about capturing the local disturbance phenomenon.

301 Closer spacing between potential host trees facilitates dispersal

- $_{302}$ If this drives mortality patterns, then we'd expect the count of ponderosa pine trees, accounting for other
- variables, to have a strong positive effect.

304 Host preference for large trees

- 305 If this drives mortality patterns, then we'd expect the quadratic mean diameter of ponderosa pine trees,
- accounting for other variables, to have a strong positive effect.

Denser forests augment pheromone communication

308 If this drives mortality patterns, then we'd expect the count of all trees, accounting for other variables, to

have a strong positive effect.

312

$_{310}$ Tree crowding leads to greater average water stress per tree

311 If this drives mortality patterns, then we'd expect the quadratic mean dimater of all trees, accounting for

313 Interaction between host density and host size

other factors, to have a strong positive effect.

A positive coefficient would indicate a combined effect of WPB preference for large trees and nearby host availability.

316 Interaction between all tree density and all tree size

A positive coefficient would indicate a combined effect of tree crowding and pheromone communication enhancement.

Interactions with climatic water deficit

Are any of the above mechanisms exacerbated by water stress of the trees?

321 Important considerations

³²² Cumulative effect of elevated insect activity, as mortality was spread out over 5 years and we surveyed at the end.

324 Future directions

My goal is to tease apart the relative role of environmental drivers versus behavioral drivers of bark beetleinduced tree mortality. I think teasing these apart will help with inference about the mechanism underlying
the effect of forest structure on disturbance severity. Crowded forests means trees are both water stressed
and are closer targets for new attacks [i.e., shorter dispersal needed to attack the next tree], and I think
comparing the "voronoi polygon area" effect with the "spatial covariance of mortality kernel" effect across
sites will tell us whether it's the water stress or the smaller dispersal requirements driving mortality patterns.
A big voronoi polygon area effect and a short covariance kernel tells us that it's a water stress effect— a
crowded tree gets attacked regardless of whether nearby trees were attacked. A small voronoi polygon area

- effect and a long covariance kernel tells us that the mortality is patterned more based on there being spillover
- from nearby attacked neighbors instead of how crowded any given tree is. I expect we might see different
- relative magnitudes of voronoi polygon area and covariance kerenel effects depending on CWD.

36 References

- Baldwin BG, Thornhill AH, and Freyman WA et al. 2017. Species richness and endemism in the native flora
- of California. American Journal of Botany 104: 487–501.
- 339 Clevers J and Gitelson A. 2013. Remote estimation of crop and grass chlorophyll and nitrogen content using
- 340 red-edge bands on Sentinel-2 and -3. International Journal of Applied Earth Observation and Geoinformation
- **23**: 344–51.
- ³⁴² Coops NC, Johnson M, Wulder MA, and White JC. 2006. Assessment of QuickBird high spatial resolution
- imagery to detect red attack damage due to mountain pine beetle infestation. Remote Sensing of Environment
- **103**: 67–80.
- 545 DJI. 2015a. Zenmuse X3 Creativity Unleashedhttps://www.dji.com/zenmuse-x3/info. Viewed 4 Mar 2019.
- ³⁴⁶ DJI. 2015b. DJI The World Leader in Camera Drones/Quadcopters for Aerial Photographyhttps://www.
- dji.com/matrice100/info. Viewed 4 Mar 2019.
- Easy DM. 2018. Map Pilot for DJIhttps://itunes.apple.com/us/app/map-pilot-for-dji/id1014765000?mt=8.
- ³⁴⁹ Viewed 4 Mar 2019.
- Eysn L, Hollaus M, and Lindberg E et al. 2015. A Benchmark of Lidar-Based Single Tree Detection Methods
- Using Heterogeneous Forest Data from the Alpine Space. Forests 6: 1721-47.
- Farr TG, Rosen PA, and Caro E et al. 2007. The Shuttle Radar Topography Mission. Reviews of Geophysics
- 353 **45**.
- Fettig CJ. 2012. Chapter 2: Forest health and bark beetles. In: Managing Sierra Nevada Forests. PSW-
- 355 GTR-237. USDA Forest Service.
- Fettig CJ, Mortenson LA, Bulaon BM, and Foulk PB. 2019. Tree mortality following drought in the central
- and southern Sierra Nevada, California, U.S. Forest Ecology and Management 432: 164-78.
- Flint LE, Flint AL, Thorne JH, and Boynton R. 2013. Fine-scale hydrologic modeling for regional landscape
- applications: The California Basin Characterization Model development and performance. Ecological Processes

- 360 **2**: 25.
- Floyd ML, Clifford M, and Cobb NS et al. 2009. Relationship of stand characteristics to drought-induced
- mortality in three Southwestern piñonJuniper woodlands. Ecological Applications 19: 1223–30.
- ³⁶³ Gitelson A and Merzlyak MN. 1994. Spectral Reflectance Changes Associated with Autumn Senescence of
- ³⁶⁴ Aesculus hippocastanum L. and Acer platanoides L. Leaves. Spectral Features and Relation to Chlorophyll
- Estimation. Journal of Plant Physiology 143: 286–92.
- Hayes CJ, Fettig CJ, and Merrill LD. 2009. Evaluation of Multiple Funnel Traps and Stand Characteristics
- for Estimating Western Pine Beetle-Caused Tree Mortality. Journal of Economic Entomology 102: 2170-82.
- Hijmans RJ, Etten J van, and Sumner M et al. 2019. Raster: Geographic Data Analysis and Modeling.
- Hunziker P. 2017. Velox: Fast Raster Manipulation and Extraction.
- Jakubowski MK, Li W, Guo Q, and Kelly M. 2013. Delineating Individual Trees from Lidar Data: A
- ³⁷¹ Comparison of Vector- and Raster-based Segmentation Approaches. Remote Sensing 5: 4163–86.
- Kane VR, North MP, and Lutz JA et al. 2014. Assessing fire effects on forest spatial structure using a fusion
- of Landsat and airborne LiDAR data in Yosemite National Park. Remote Sensing of Environment 151:
- 374 89-101.
- 375 Kuhn M. 2008. Building Predictive Models in R Using the caret Package. Journal of Statistical Software 28:
- 1-26.
- Larson AJ and Churchill D. 2012. Tree spatial patterns in fire-frequent forests of western North America,
- 378 including mechanisms of pattern formation and implications for designing fuel reduction and restoration
- treatments. Forest Ecology and Management 267: 74–92.
- 280 Li W, Guo Q, Jakubowski MK, and Kelly M. 2012. A New Method for Segmenting Individual Trees from the
- Lidar Point Cloud. Photogrammetric Engineering & Remote Sensing 78: 75–84.
- ³⁸² Meyer F and Beucher S. 1990. Morphological segmentation. Journal of Visual Communication and Image
- Representation 1: 21-46.
- Micasense. 2015. MicaSensehttps://support.micasense.com/hc/en-us/articles/215261448-RedEdge-User-Manual-PDF-Downlo
- ³⁸⁵ Viewed 4 Mar 2019.
- 386 Millar CI and Stephenson NL. 2015. Temperate forest health in an era of emerging megadisturbance. Science

- 387 **349**: 823–6.
- Negrón JF, McMillin JD, Anhold JA, and Coulson D. 2009. Bark beetle-caused mortality in a drought-affected
- ponderosa pine landscape in Arizona, USA. Forest Ecology and Management 257: 1353–62.
- North MP, Stephens SL, and Collins BM et al. 2015. Reform forest fire management. Science 349: 1280-1.
- Pau G, Fuchs F, and Sklyar O et al. 2010. EBImagean R package for image processing with applications to
- cellular phenotypes. *Bioinformatics* **26**: 979–81.
- Pebesma E, Bivand R, and Racine E et al. 2019. Sf: Simple Features for R.
- Plowright A. 2018. ForestTools: Analyzing Remotely Sensed Forest Data.
- Popescu SC and Wynne RH. 2004. Seeing the Trees in the Forest: Using Lidar and Multispectral Data
- Fusion with Local Filtering and Variable Window Size for Estimating Tree Height. PHOTOGRAMMETRIC
- 397 ENGINEERING: 16.
- R Core Team. 2018. R: A Language and Environment for Statistical Computing. Vienna, Austria: R
- Foundation for Statistical Computing.
- ⁴⁰⁰ Raffa KF, Aukema BH, and Bentz BJ et al. 2008. Cross-scale Drivers of Natural Disturbances Prone to
- 401 Anthropogenic Amplification: The Dynamics of Bark Beetle Eruptions. BioScience 58: 501–17.
- 402 Rouse W, Haas RH, Deering W, and Schell JA. 1973. MONITORING THE VERNAL ADVANCEMENT
- 403 AND RETROGRADATION (GREEN WAVE EFFECT) OF NATURAL VEGETATION. Greenbelt, MD,
- 404 USA: Goddard Space Flight Center.
- Roussel J-R. 2019. lidRplugins: Extra functions and algorithms for lidR package.
- Roussel J-R, documentation) DA(the, and improved catalog features) FDB(bugs, and lassnags) ASM(. 2019.
- 407 lidR: Airborne LiDAR Data Manipulation and Visualization for Forestry Applications.
- Shin P, Sankey T, Moore M, and Thode A. 2018. Evaluating Unmanned Aerial Vehicle Images for Estimating
- Forest Canopy Fuels in a Ponderosa Pine Stand. Remote Sensing 10: 1266.
- 410 Stephenson N. 1998. Actual evapotranspiration and deficit: Biologically meaningful correlates of vegetation
- distribution across spatial scales. Journal of Biogeography 25: 855–70.
- USDAFS. 2019. Press Release: Survey finds 18 million trees died in California in 2018https://www.fs.usda.
- 413 gov/Internet/FSE DOCUMENTS/FSEPRD609321.pdf. Viewed 22 Feb 2019.
- Vega C, Hamrouni A, and El Mokhtari S et al. 2014. PTrees: A point-based approach to forest tree extraction

- from lidar data. International Journal of Applied Earth Observation and Geoinformation 33: 98–108.
- Wood SN, Pya N, and Säfken B. 2016. Smoothing Parameter and Model Selection for General Smooth
- 417 Models. Journal of the American Statistical Association 111: 1548–63.
- 418 Young DJN, Stevens JT, and Earles JM et al. 2017. Long-term climate and competition explain forest
- mortality patterns under extreme drought. Ecology Letters 20: 78–86.
- Zhang W, Qi J, and Wan P et al. 2016. An Easy-to-Use Airborne LiDAR Data Filtering Method Based on
- ⁴²¹ Cloth Simulation. Remote Sensing 8: 501.